

X-ray Emissions from Three-dimensional Magnetohydrodynamic Coronal Accretion Flows

Norita Kawanaka,¹ Yoshiaki Kato,² and Shin Mineshige³

¹ Research Center for the Early Universe, Graduate School of Science,
The University of Tokyo, 7-3-1, Hongo, Bunkyo-ku, Tokyo, 113-0033, Japan

² Institute of Space and Astronautical Science, JAXA, 3-1-1, Yoshinodai, Sagami-hara, Kanagawa, 229-8510, Japan

³ Department of Astronomy, Kyoto University, Oiwake-cho, Kitashirakawa, Sakyo-ku, Kyoto, 606-8502, Japan
E-mail(NK): norita@resceu.s.u-tokyo.ac.jp

ABSTRACT

In explaining the spectral properties of active galactic nuclei (AGNs) and X-ray binaries, it is often assumed that they consist of a geometrically thin, optically thick disk and hot, optically thin corona surrounding the thin disk. As for a model of a corona, we adopt the simulation data of three-dimensional, non-radiative MHD accretion flows calculated by Kato and coworkers, while for a thin disk we assume a standard type disk. We perform Monte Carlo radiative transfer simulations in the corona, taking into account the Compton scattering of the soft photons from the thin disk by hot thermal electrons and coronal irradiation heating of the thin disk, which emits blackbody radiation. By adjusting the density parameter of the MHD coronal flow, we can produce the emergent spectra which are consistent with those of typical Seyfert galaxies. Moreover, we find rapid time variability in X-ray emission spectra, originating from the density fluctuation produced by the magnetorotational instability in the MHD corona.

KEY WORDS: accretion, accretion disk – black hole physics – radiative transfer – X-rays: general

1. Introduction

Accreting black holes, such as active galactic nuclei (AGNs) and black hole binaries (BHs) during their very-high spectral state [state with luminosities around a few tenths of the Eddington limit (L_{Edd})], show the radiation spectra dominated by two components; the thermal bump in UV/soft X-ray band and the power-law emission with a spectral index of $\alpha \sim 1$ in the X-ray band (possibly with a high energy cutoff around MeV). In addition, iron fluorescent line emission feature ($\sim 6 - 7\text{keV}$) and reflection hump (a few tens-100keV) are often observed. These components are often explained by the disk-corona model (Liang & Price 1977; Bisnovatyi-Kogan & Blinnikov 1977; Haardt & Maraschi 1991, 1993). In this model, the accretion flow consists of geometrically thin, optically thick accretion disk whose structure is studied by Shakura & Sunyaev (1973), and hot, optically thin corona surrounding the disk. The thermal bump is believed as the thermal emission from the optically thick disk, and the power-law component is interpreted to be formed by photons which are emitted from the disk and Compton up-scattered by hot electrons in the corona. So far, however, most of theoretical corona models assume that the coronal structure is steady in time and then the spectral energy distribution is also steady. Such feature

cannot explain the highly time-variable spectral behavior of accreting black holes.

On the other hand, in understanding the structure and dynamics of accretion flows, the magnetohydrodynamic (MHD) approach is indispensable, since Balbus & Hawley (1991) rediscovered the magnetorotational instability (MRI) as the fundamental mechanism of angular momentum transfer in accretion disks. Detailed dynamical features of MHD accretion flows have been investigated via global three-dimensional numerical simulations by many authors (Matsumoto 1999; Stone & Pringle 2001; Machida et al. 2001; Hawley & Krolik 2001, 2002; Machida & Matsumoto 2003; Armitage & Reynolds 2003; De Villiers et al. 2003; Gammie et al. 2003; Igumenshchev et al. 2003). In those accretion flows simulated in their studies, the dissipated energy would not be radiated away efficiently, because of their low density, and be advected inward to the central black hole (Ichimaru 1977; Narayan & Yi 1994; Abramowicz et al. 1995; Kato et al. 1998). Such accretion flows are referred to as “radiative inefficient accretion flows” (RIAFs). The RIAF model is believed to fit the emergent spectrum of Sagittarius A*, some authors have calculated the time dependent radiation spectra predicted from simulated MHD accretion flows with the aim to reproduce the observed behavior of Sgr A* (Hawley &

Balbus 2002; Goldstone et al. 2005; Ohsuga et al. 2005; Moscibrodzka et al. 2007).

In this study, we adopted the three-dimensional simulation data of RIAFs by Kato et al. (2004, hereafter KMS04) as a model of time-dependent, hot and optically thin corona, and calculate for the first time the emergent spectra of disk-corona accretion flow systems. We assume that the optically thick, geometrically thin disk is embedded in the corona, and that this disk is emitting soft photons with thermal spectrum. The interactions other than radiative processes, such as mass evaporation/condensation or heat conduction, are neglected, for simplicity. We perform three-dimensional Monte Carlo radiative transfer simulations to properly calculate the radiation processes and the emergent spectra predicted from this disk corona model (for the detail see Kawanaka et al. 2008).

2. Model and Calculation Method

2.1. Overview of the Adopted MHD Corona Model

KMS04 investigated the evolution of a torus threaded by weak localized poloidal magnetic fields by performing the three-dimensional MHD simulation. They solved the basic equations of the resistive MHD in the cylindrical coordinates, (r, ϕ, z) . The calculation was started with a rotating torus in hydrostatic balance located around $r = r_0 = 40r_S$. The entire computational box size is $0 \leq r \leq 200r_S$, $0 \leq \phi \leq 2\pi$, and $-50r_S \leq z \leq 50r_S$, and they simulated a full 360° domain (see KMS04 and Kato 2004 for more detail).

The simulated MHD flow has almost steady structure, but is slightly oscillating because of the turbulence driven by MRI, and geometrically thick density distribution is produced. In this quasi-steady accretion flow, the density profile is $\rho \propto r$ in the inner part ($r < 20r_S$), while $\rho \propto r^{-1}$ in the outer part ($r > 20r_S$) (see Fig. 4 in KMS04). We use this quasi-steady density distribution as well as the ion temperature distribution in modeling the corona in which hot thermal electrons up-scatter the soft photons emerging from the cold disk virtually located in the equatorial plane. The data of physical properties are given at each point in the simulation box associated with Cartesian coordinates (x, y, z) , in which the black hole is located at the origin of the coordinate axes, the z -axis is set to be the rotation axis of the accretion flow, and the x - y plane corresponds to the equatorial plane. We employ Cartesian grids with numbers $(N_x, N_y, N_z) = (101, 101, 101)$ of cells. The size of the calculating box is $2X \times 2Y \times 2Z$, where we set $(X, Y, Z) = (99.9r_S, 99.9r_S, 99.9r_S)$.

In the MHD simulations with no radiative loss the density is given as non-dimensional number $\tilde{\rho}$ with the normalization factor ρ_0 , which is treated a free parameter in our calculation. Basically the coronal density is

determined by evaporation of the disk gas, but here we determine ρ_0 so that the spectral features predicted from the corona with such density agree with the observations.

As for the electron temperature, we should note that it is not the same as the proton temperature, which is directly derived from the simulation. Actually the electrons in a corona are cooled via inverse Compton scattering, and so should have a lower temperature in the realistic situation. We can evaluate the electron temperature, T_e , through the energy balance of the electrons between Coulomb collisions with ions and radiative cooling,

$$\int_{-Z}^Z \int_{r_{\text{in}}}^{r_{\text{out}}} \lambda_{ie} 2\pi r dr dz = \int L_C(\nu; r_{\text{in}} \leq r \leq r_{\text{out}}) d\nu. \quad (1)$$

Here λ_{ie} is the energy transfer rate from ions to electrons (Stepney & Guilbert 1983) and $L_C(\nu)$ is the coronal luminosity at frequency ν . In the present study, we divide the corona into three regions ($0 < r \leq 10r_S$, $10r_S < r \leq 30r_S$, and $30r_S < r$; $(r_{\text{in}}, r_{\text{out}}) = (0, 10r_S)$, $(10r_S, 30r_S)$ and $(30r_S, \infty)$) for simplicity, and suppose that the electrons in the accretion flow in each region have the temperature which is independent of the radius r and the altitude z . The coronal luminosity, L_C , is obtained by Monte Carlo simulations (see next subsection) for a guess value of T_e . Since this T_e does not always satisfy Eq. (1), we should do some iterations to calculate the appropriate electron temperature and the emergent spectrum.

2.2. Radiative Transfer Simulations

In our calculation, as noted above, a cold and geometrically thin disk that produces blackbody radiation is assumed artificially. When irradiation flux, F_{irr} , by the corona is strong enough to heat the disk surface at a certain radius, the radiation temperature there should be enhanced from the intrinsic temperature derived from the standard disk model. In the following calculation we set $r_{\text{in}} = 3r_S$, $\dot{M}_{\text{disk}} = 10^{-3} \dot{M}_{\text{Edd}}$ (with $\dot{M}_{\text{Edd}} = 10L_{\text{Edd}}/c^2$) and the mass of a central black hole to be $M = 10^8 M_\odot$, which is believed to be the typical value for AGNs. Thus, the normalized time corresponds to $\tilde{t} \cong r_S/c = 10^3 \text{sec}$.

The method of the Monte Carlo simulation is based on Pozdnyakov et al. (1977). In order to efficiently calculate the emergent spectra, we introduce a photon weight w . When emerged from the disk we set that each photon has the weight of $w_0 = 1$, and then we calculate the escape probability, P_0 . The escape probability of a photon after i -th scattering (for $i \geq 1$), P_i , is evaluated as

$$P_i = \exp \left(- \int \left[\frac{\rho(x_i, y_i, z_i)}{m_p} \right] \sigma_{\text{KN}}(x_i, y_i, z_i) dl \right), \quad (2)$$

where $(x, y, z) = (x_0, y_0, 0)$ corresponds to the point on the equatorial plane (i.e. the disk plane), in which the thermal soft photons are generated, (x_i, y_i, z_i) is the

point where a photon is subject to the i -th scattering, m_p is the proton mass, σ_{KN} is the Klein-Nishina cross section (Rybicki & Lightman 1979), and the integral of dl should be done along the photon direction there from the point (x_i, y_i, z_i) to the boundary of the calculating box. The quantity of $w_0 P_0$ represents the transmitted portion of photons and is recorded to calculate the penetrated spectrum if the path of the photon does not cross with the equatorial plane, and will no longer continue to be counted and will be regarded to be absorbed by the disk. As for the remaining portion of a photon, its weight becomes $w_1 = w_0(1 - P_0)$. The transmitted portion of photons after i -th scattering, $w_i P_i$ is recorded to calculate the emergent spectrum, and the remaining portion, $w_i(1 - P_i)$, undergoes the $(i + 1)$ -th scattering. This calculation is continued until the weight w_i becomes sufficiently small ($w_i \ll 1$) or the path of the remaining photon crosses the equatorial plane, regarding to be absorbed by the disk.

3. Results

First, we show the emergent spectra from the accretion disk with MHD coronal flow with various density parameters for the corona in Fig. 1. The adopted density parameters ρ_0 for the corona are $\rho_0 = 5.1 \times 10^{-15}$, 1.6×10^{-14} , and $5.1 \times 10^{-14} \text{g cm}^{-3}$. These values correspond to the number density of $\sim 10^9 \text{cm}^{-3}$. Such density is consistent with some corona models (see Liu et al. 2002, 2003). Due to the inverse Compton scattering in the corona, the power-law component with the spectral index of $\alpha \sim 1 - 2$ ($F_\nu \propto \nu^{-\alpha}$) appears in the higher energy band. In the calculated spectra, we cannot find a bump-like structure clearly in the UV/soft X-ray band which is usually seen in typical spectra of AGNs. As ρ_0 increases, the total luminosities increases, while the power-law index decreases. The corona with higher density (especially with higher scattering optical depth) would irradiate the underlying disk with higher energy flux because larger number of photons originated from the disk would gain the energy and be backscattered. The the disk is heated by the corona and so the energy flux of the seed photon field would increase. This is why the total luminosity rises with the coronal density.

In Table 1 we summarize the scattering optical depths τ (evaluated by integrating the scattering opacity over the z -direction from the equatorial plane), the Compton y parameters of the corona (averaged in each region), and the spectral indices of the power law component estimated from the calculation results for 3 density parameters. The MHD simulation of coronal flow was started from the initial condition of a magnetized torus located around at $r \sim 40r_S$. The radius of maximum gas density (and of maximum τ) decreases inward with time and stays around $r \sim 20r_S$. According to the theory of unsat-

urated inverse Compton scattering, the power-law index of the Comptonized emission component depends on the plasma density and temperature through this equation:

$$\alpha = -\frac{3}{2} + \sqrt{\frac{9}{4} + \frac{4}{y}}. \quad (3)$$

Here $y \equiv (4k_B T/m_e c^2)\tau$ is the Compton y -parameter (Rybicki & Lightman 1973), where T and τ are the temperature and Thompson optical depth of the corona, respectively. The spectral indices derived from this equation using y -parameters in Table 1 do not always agree with those estimated from the spectra. This is because τ and T_{cor} have spatial distributions and we cannot evaluate y -parameter of the corona uniquely.

In our calculation, ρ_0 is determined so as to reproduce the observation. By tuning the coronal density parameter, we can reproduce the luminosity of the power-law component which is as intense as that of the thermal component originated from the optically thick disk. Such feature is typical in Seyfert galaxies. However, the coronal temperature cannot be chosen freely but should be determined by imposing the energy balance of the electrons between Coulomb collisions and the cooling via inverse Compton scattering, as we have done. Nevertheless the resulting coronal temperature is substantially reduced from the plasma temperature derived by the simulation ($\sim 10^{13}$ K) to $\sim 10^9$ K, which makes the high energy cutoff of computed spectra consistent with observations.

The spectral variation caused by the time variation of MHD coronal flow structure is shown in Fig. 2. In the highest energy range ($\geq 10^{18}$ Hz) the spectra show fluctuations because of poor photon statistics. As for the soft X-ray band (with $\log \nu \simeq 17 - 18$) where the spectra show a smooth power-law shape, the spectral index slightly changes with time, and then the X-ray flux fluctuates a little (see also Fig. 3). According to the MHD simulation on which our radiative transfer calculations are based, the three-dimensional structure of the coronal accretion flow is fluctuating everywhere in each timestep. On the other hand, the spectral index depends on the distribution of y -parameter of the corona, as we note in the last subsection. So we can conclude that the fluctuations of the spectral indices of the computed spectra in Fig. 2 reflect the fluctuation of y , which comes from the density fluctuations (which is supposed to be due to MRI) in the coronal flow.

Fig. 3. shows the X-ray lightcurve derived from our simulations. From this plot we can see that the X-ray luminosity from our disk-corona system can change by factors of a few tens of percent on timescales of the orbital period at the last stable orbit ($r = 3r_S$), i.e. about $10^3(M/10^8)M_\odot$ sec. In the whole calculation we do not vary the properties of the soft photon source (i.e. the un-

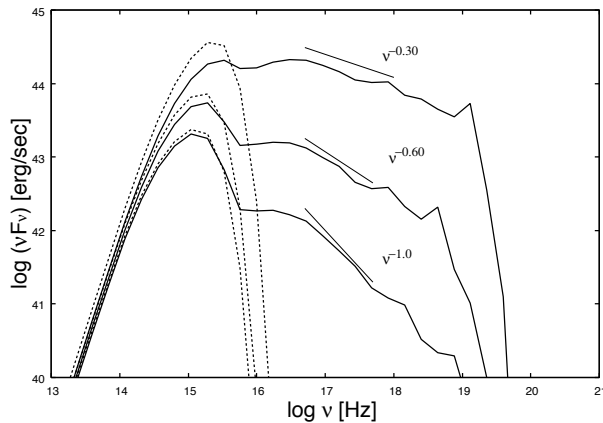


Fig. 1. Broadband spectra from a disk at the accretion rate of $10^{-3}M_{\text{Edd}}$ and a MHD coronal flow around a black hole of $10^8 M_{\odot}$ with the density normalization parameters 5.1×10^{-15} , 1.6×10^{-14} and $5.1 \times 10^{-14} \text{ g cm}^{-3}$ *solid lines*. The spectra of the seed photons (including those from the cold disk and the reflection component; *dashed lines*) are also shown for the comparison. The short solid lines near the spectra show the power-law fit of νF_{ν} .

Table 1. Coronal properties

$\rho_0 \text{ (g cm}^{-3}\text{)}$	region	$T_{\text{cor}} \text{ [K]}$	τ	y	α
5.1×10^{-14}	$0 < r < 10r_S$	$\sim 5.2 \times 10^9$	~ 0.2	~ 0.5	~ 1.30
	$10r_S < r < 30r_S$	$\sim 3.4 \times 10^9$	~ 0.9	~ 3	
	$30r_S < r$	$\sim 7.6 \times 10^8$	~ 0.7	~ 0.5	
1.6×10^{-14}	$0 < r < 10r_S$	$\sim 5.2 \times 10^9$	~ 0.05	~ 0.2	~ 1.60
	$10r_S < r < 30r_S$	$\sim 3.4 \times 10^9$	~ 0.25	~ 0.55	
	$30r_S < r$	$\sim 7.5 \times 10^8$	~ 0.2	~ 0.1	
5.1×10^{-15}	$0 < r < 10r_S$	$\sim 5.2 \times 10^9$	~ 0.02	~ 0.05	~ 2.00
	$10r_S < r < 30r_S$	$\sim 3.4 \times 10^9$	~ 0.09	~ 0.15	
	$30r_S < r$	$\sim 7.6 \times 10^8$	~ 0.07	~ 0.03	

derlying cold disk). This variation which we obtained is due to the density fluctuation (and accompanying temperature fluctuation) of the coronal flow.

4. Discussion and Conclusion

We have calculated the emergent spectra and their time variabilities predicted based on the disk-corona model, in which a cold standard disk at the equatorial plane is sandwiched by a hot coronal flow. As for the structure and dynamics of the corona we use the three-dimensional MHD simulation data by Kato (2004). The power-law indices and the cutoff energy scales of the calculated spectra are roughly in agreement with those of Seyfert galaxies. Moreover, we find significant variability of the power-law X-ray emission. The power-law X-ray emission flux predicted from our model changes by a few tens of percent on timescales of the orbital period near the last stable orbit, which is about $10^3(M/10^8 M_{\odot})$ sec. This variability comes purely from the fluctuation of the coronal flow around $r \sim 20r_S$, where the scattering optical depth of the coronal flow attains its largest value in its

structure. This fluctuation is driven by the turbulence as a result of MRI.

we should mention the interaction between the corona and the underlying disk. In the transition zone between the hot corona and the cold disk where density and temperature abruptly change, the heat conduction and the mass evaporation would be important as the mass and energy exchanging processes (Meyer & Meyer-Hofmeister 1994; Liu et al. 2002). Evaporation of photospheric material was actually shown to be essential in the context of solar flares (see e.g. Yokoyama & Shibata 1994). By including these effects in the simulation we will be able to obtain a more realistic model of the coronal structure and dynamics. To what extent the disk-corona structure can extend to the inner region is important when we consider the relativistic skewing of the iron line emission profile because most of the observations of iron line profiles imply that the iron fluorescence line photons are emitted from around/inside the last stable orbit. The detailed analysis of such disk-corona interactions and their observational implications are left as a future work.

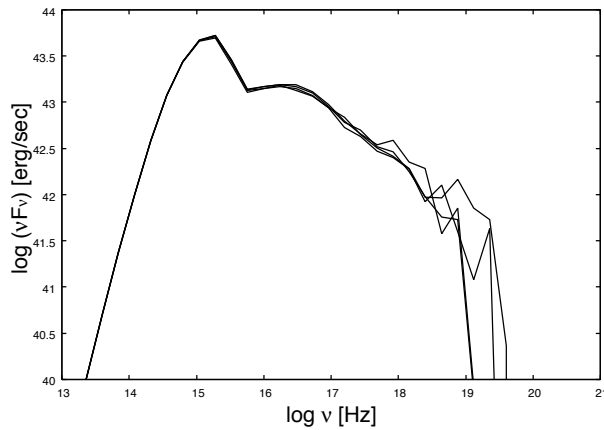


Fig. 2. Spectral variation of the Comptonized emission predicted from the standard disk with a MHD coronal flow around a black hole of $10^8 M_\odot$. Here we set the density parameter as $1.6 \times 10^{-14} \text{g cm}^{-3}$.

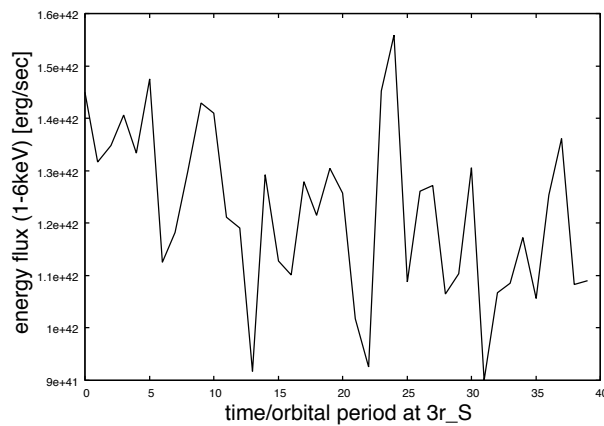


Fig. 3. Time variation of the X-ray luminosity (1-6keV). Here we set the density parameter as $1.6 \times 10^{-14} \text{g cm}^{-3}$.

Finally, we mention about the application of our corona model for black hole binaries in their low/hard state (LHS), which appears under relatively low accretion rates. In such situations, a geometrically thick and optically thin accretion flow will appear in the innermost regions of the disk near the central black hole, while the geometrically thin and optically thick disk (i.e. standard disk) is truncated at a larger radius. This accretion flow is called as ADAF and the structure and spectral behavior of such accretion flow has been continuously investigated (Ichimaru 1977; Narayan & Yi 1994). In those theoretical models, hard power-law X-ray emissions are considered to be generated via inverse Compton scattering in the innermost hot accretion flow, and the seed photons of Comptonization are thought to be supplied by synchrotron emission from electrons in the inner region. Recently, however, Suzaku revealed the broadband X-ray spectra of black hole binaries such as GRO J1655-40 (Takahashi et al. 2008) and Cyg X-1 (Makishima et al. 2008) and it has been realized that they can be fitted by “double compton” model. In that model hard X-ray

emission is produced in hot Comptonizing corona which has two characteristic optical depths, and the seed photons are provided by a geometrically thin and optically thick disk. This radiative process is different from that considered in the original ADAF model. Moreover, the fact that two coronal components which have different optical depths implies that the corona has a spatial distribution in the optical depth. These features are well reproduced in our corona model. As for the spectral variability, the observed spectrum becomes softer in the high flux phase, which implies the lower coronal temperature, and the underlying disk is supposed to remain unchanged. The coronal temperature should be lowered if Compton upscatterings occur efficiently and vice versa, so this observation can be interpreted as follows: X-ray luminosity varies solely because of the oscillation in the Comptonizing coronal flow while the underlying disk which emits seed photons into the corona does not need to vary. This interpretation is fully consistent with our corona model. In the forthcoming paper (Kawanaka et al. in prep), we explain the X-ray spectrum and its

variability and interpret the observational data theoretically with our MHD corona model.

References

- Abramowicz, M. A., Chen, X., Kato, S., Lasota, J.-P. & Regev, O. 1995, *ApJ*, 438, L37
- Armitage, P. J. & Reynolds, C. S. 2003, *MNRAS*, 341, 1041
- Balbus, S. A. & Hawley, J. F. 1991, *ApJ*, 376, 214
- Bisnovatyi-Kogan, G. S. & Blinnikov, S. I. 1977, *A&A*, 59, 111
- De Villiers, J. -P., Hawley, J. F. & Krolik, J. H. 2003, *ApJ*, 599, 1238
- Gammie, C. F., McKinney, J. C. & Toth, G. 2003, *ApJ*, 589, 444
- Haardt, F. & Maraschi, L. 1991, *ApJ*, 380, L51
- Haardt, F. & Maraschi, L. 1993, *ApJ*, 413, 507
- Hawley, J. F. & Krolik, J. H. 2001, *ApJ*, 548, 348
- Hawley, J. F. & Krolik, J. H. 2002, *ApJ*, 566, 164
- Ichimaru, S. 1977, *ApJ*, 214, 840
- Igumenshchev, I. V., Narayan, R. & Abramowicz, M. A. 2003, *ApJ*, 592, 1042
- Kato, S., Fukue, J. & Mineshige, S. 1998, *Black-Hole Accretion Disks* (Kyoto: Kyoto Univ. Press)
- Kato, Y. 2004, *PASJ*, 56, 931
- Kato, Y., Mineshige, S. & Shibata, K. 2004, *ApJ*, 605, 307 (KMS04)
- Kawanaka, N., Mineshige, S. & Iwasawa, K. 2005, *ApJ*, 635, 167
- Kawanaka, N., Kato, Y. & Mineshige, S. 2008, *PASJ*, 60, 399
- Liang, E. P. T & Price, R. H. 1977, *ApJL*, 218, 247
- Liu, B. F., Mineshige, S., Meyer, F., Meyer-Hofmeister, E. & Kawaguchi, T. 2002, *ApJ*, 575, 117
- Machida, M. & Matsumoto, R. 2003, *ApJ*, 585, 429
- Machida, M., Matsumoto, R. & Mineshige, S. 2001, *PASJ*, 53, L1
- Makishima, K., Takahashi, H., Yamada, S., Done, C., Kubota, A., Dotani, T., Ebisawa, K., Itoh, T., Kitamoto, S., Negoro, H., Ueda, Y. & Yamaoka, K. 2008, *PASJ*, 60, 585
- Matsumoto, R. 1999, in *Numerical Astrophysics*, ed. S. M. Miyama, K. Tomisaka & T. Hanawa (Boston: Kluwer), 195
- Meyer, F. & Meyer-Hofmeister, E. 1994, *A&A*, 288, 175
- Moscibrodzka, M., Proga, D., Czerny, B. & Siemiginowska, A. 2008, *ApJ*, 679, 626
- Narayan, R. & Yi, I. 1994, *ApJ*, 428, L13
- Ohsuga, K., Kato, Y. & Mineshige, S. 2005, *ApJ*, 627, 782
- Pozdnyakov, L. A., Sobol, I. M. & Sunyaev, R.A. 1977, *Soviet Astron.*, 21, 708
- Rybicki, G. B., & Lightman, A. P. 1979, *Radiative Processes in Astrophysics* (New York: Wiley)
- Shakura, N. I. & Sunyaev, R. A. 1973, *A&A*, 24, 337
- Stone, J. M. & Pringle, J. E. 2001, *MNRAS*, 322, 461
- Takahashi, H. et al., 2008, *PASJ*, 60, 69
- Yokoyama T. & Shibata, K. 1994, *ApJ*, 436, L197